

Silver Nanoparticles Decorated on Graphene Oxide Sheets for Electrochemical Detection of Ascorbic Acid(AA) in Human Urine Sample

Karthika pichaimuthu², Murugan Keerthi¹, Shen-Ming Chen^{1,*}, Tse-Wei Chen¹, Chaochin Su²

¹ Department of Chemical Engineering and Biotechnology, National Taipei University of Technology, No.1, Section 3, Chung-Hsiao East Road, Taipei 106, Taiwan.

² Institute of Organic and Polymeric Materials, National Taipei University of Technology, Taipei 10608, Taiwan

*E-mail: smchen78@ms15.hinet.net, smchen1957@gmail.com

Received: 13 April 2018 / Accepted: 3 June 2018 / Published: 5 July 2018

Here, we report a non-enzymatic Silver nanoparticle-decorated graphene oxide (Ag NPs-GO) nanocomposite based electrochemical biosensor for the detection of ascorbic acid using the ultra-sensitive electrochemical method. In this work, Ag NPs-GO nanocomposite synthesized through simple and cost-effective ultra-sonication method. As produced composite was characterized by FE-SEM, TEM, EDX, FT-IR, XRD, EIS and electrochemical methods. The electrochemical behavior of ascorbic acid at the surface of Ag NPs-GO nanocomposite modified screen-printed carbon electrode (SPCE) was investigated by cyclic voltammetry (CV) technique while ascorbic acid sensing was performed by Differential pulse voltammetry method. The as-developed biosensor exhibited lower detection limit of 25 nM and the sensitivity is $1.71 \mu\text{A } \mu\text{M}^{-1} \text{ cm}^{-2}$ ($R^2=0.997$) towards ascorbic acid in the linear range of 1–210 μM with no surface fouling was observed. To evaluate the practical application, the detection of AA performed in the real sample of human urine and vitamin C tablets to predict unknown concentrations of in the PBS pH 7.0.

Keywords: non-enzymatic biosensor; Ultra-sonication method; Ag NPs-GO nanocomposite; ascorbic acid; Electrochemical detection

1. INTRODUCTION

Ascorbic acid (AA) is commonly known as vitamin C and plays a vital role in metabolic reactions of a living organism [1]. Insufficient supply of ascorbic acid in human body causes symptoms of scurvy, cardio vascular diseases, Parkinson's disease, hypo-immunity and even cancer whilst excess of ascorbic acid results in diarrhea, hyperacidity [2-3]. Therefore, the exact detection of

ascorbic acid is significant importance in pharmaceutical industries, clinical diagnostics, and food safety [4-10]. Since, various conventional analytical methods have been developed for ascorbic acid detection such as flow injection analysis, fluorescence spectroscopy, calorimetry and high-performance liquid chromatography (HPLC) etc. [11-13]. These methods quite unsuitable due to excess time consuming, sophisticated instrumentation, sample pre-treatments and complex extraction and so on [10]. Among these methods, the electrochemical method has attracted significant attention for direct detection and quantification of ascorbic acid due to their high sensitivity, rapid analysis, simplicity, low cost and continuous real-time detection [10, 14-15]. Electrochemical detection of ascorbic acid is performed with both enzymatic and non-enzymatic sensor. Enzymatic ascorbic acid sensors associated with some drawbacks which include expensive enzymes used for surface immobilization, poor reproducibility and greatly affected by working conditions such as temperature, pH, and humidity [3]. In the non-enzymatic platform, ascorbic acid oxidation detected through using suitable electrodes [10]. In order to enhance electrochemical performance, electrodes are modified with various materials such as metal oxides, metal nanoparticles and carbon-based materials [15]. Now a day in a research field, the Graphene oxide has a great interest in electrochemical due to its unique structure and high electrical conductivity. Graphene oxide (GO) is considered as a derivative of graphene which is derived from graphite through the chemical oxidation reaction, with subsequent dispersion in water or suitable organic solvents [16]. The large amount of oxygen functional groups such as carbonyl, hydroxyl, carboxyl and epoxy groups on its surface. These functional groups allow metal nanoparticles to contact with the GO sheets through electrostatic interactions. In particular, the metal ion species stabilized by presence of carboxylic moieties on the surface of GO. Thus, the reduction takes place at the GO surface and it gives a one-step formation of metal nanoparticles to their sheets without the need for any functionalization. In order to improve further electrocatalytic activity, silver nanoparticles decorated on GO through ultra-sonication method [17-20]. Ag NPs have an extensively studied in various chemical, physical and biological studies due to their highest electrical conductivity, antibacterial properties and excellent catalytic properties [21-24]. Therefore, it is interesting to decorated Ag NPs into GO to enhance catalytic performance. We have developed non-enzymatic Ag NPs-GO Nanocomposites modified screen-printed carbon electrode for electrocatalytic oxidation of ascorbic acid.

2. EXPERIMENTAL

2.1 Materials and Instrumentations

Natural graphite powder, Sodium nitrate (NaNO_3), potassium permanganate (KMnO_4), sulfuric acid (H_2SO_4), hydrochloric acid (HCl), hydrogen peroxide (H_2O_2), silver nitrate (AgNO_3), sodium borohydride (NaBH_4) and Potassium hexa cyanoferrate(II) were purchased from Sigma-Aldrich. The SPCEs were purchased from Zensor R&D Co., Ltd., Taipei, Taiwan. CHI 1205C workstation used for the conducting electrochemical measurements with the conventional three-electrode cell. The cell consists of BAS SPCE as a working electrode (surface area 0.017 cm^2), saturated Ag/AgCl as a reference electrode and Pt wire as a counter electrode. A Powder X-ray diffraction studies conducted

in an XPERT-PRO diffractometer using Cu K α radiation ($k=1.54 \text{ \AA}$). Electrochemical impedance spectroscopy (EIS) EIM6ex Zahner used to calculate the electron transfer ability of electrode.

2.2 Synthesis of Ag NPs-GO nanocomposite

GO prepared by modified Hummers method. In order to prepare Ag NPs-GO nanocomposite, 200 mg of GO was dispersed in a solution containing 20:1 ratio of DI water and ethanol under ultra-sonication for 1 h. After that 100 mg of AgNO₃ and 10 mg of sodium borohydride solution (reducing agent) was added to above solution by drop-wise and kept it into ultra-sonicated for 1 h. the resulting Ag NPs-GO nanocomposite is washed several times with DI water and ethanol to remove the impurities and then the nanocomposite was collected by filtration using membrane filter. Finally, the obtained nanocomposite dried in vacuum oven at 50°C.

3. RESULTS AND DISCUSSION

3.1. surface morphological and elemental characterizations of Ag NPs-GO nanocomposite

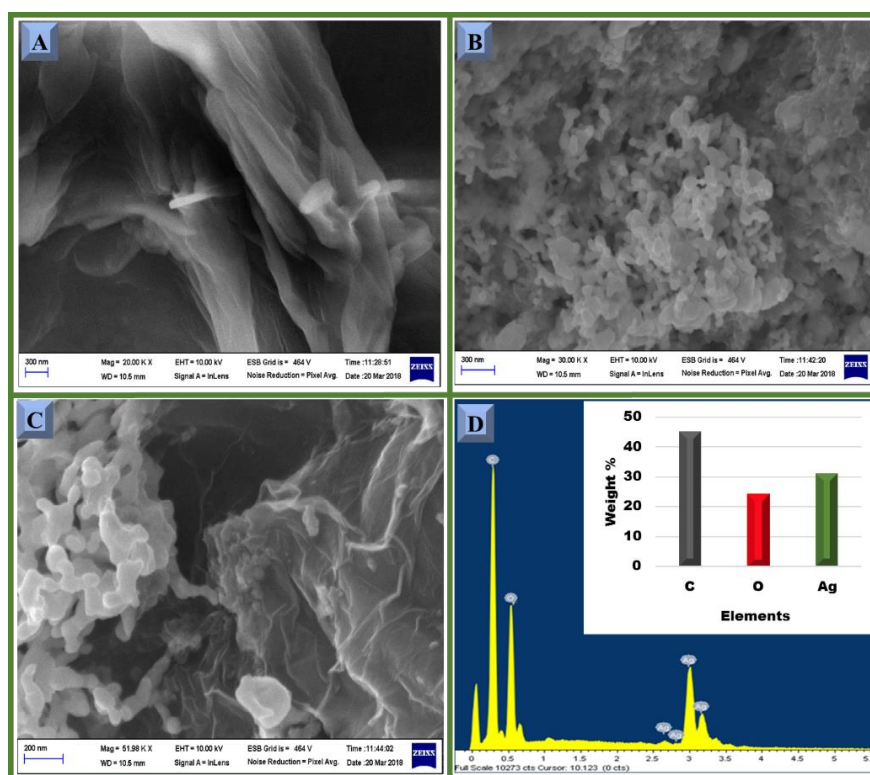


Figure 1. FE-SEM images of GO (A), Ag NPs-GO nanocomposite (B, C) and EDX spectra of nanocomposite (D).

Surface morphology and elemental composition of Ag NPs-GO nanocomposites were determined by FE-SEM and EDX. (Figure. 1A) shows smooth and thin sheet-like the structure of graphene oxide. (Figure. 1B and C) shows a representative SEM images of the Ag NPs-GO

nanocomposite. It was clearly seen that a large amount of Ag nanoparticle uniformly distributed at the GO surface. These Ag nanoparticles in the GO surface are spherical in shape and the sizes ranging from 50 to 60 nm. The existence of C, O, Ag elements in Ag NPs-GO nanocomposites revealed the formation of Ag nanoparticles on the surfaces of GO sheets which confirmed through the energy-dispersive X-ray spectrum results (EDX) (Figure. 1D).

3.2 PXRD and FTIR studies of Ag NPs-GO nanocomposite

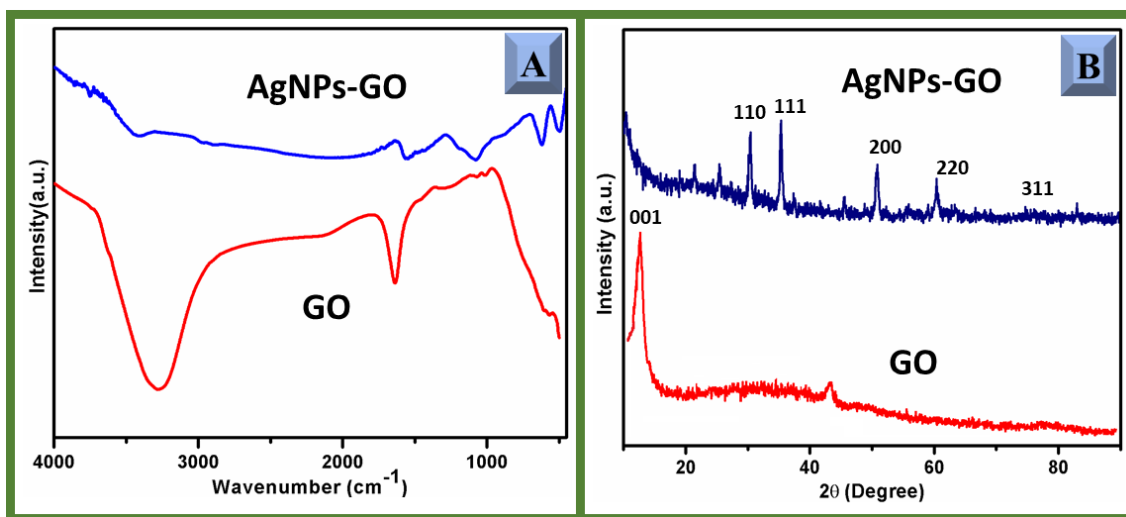


Figure 2. FTIR spectra (A). PXRD spectrum of nanocomposite (B).

(Figure 2A) displays the FT-IR spectra of GO and Ag NPs-GO nanocomposites. GO spectrum was observed at 3400, 1650 and 1050 cm^{-1} due to stretching vibration of C-OH (hydroxyl), the stretching vibration of C=O, and C-O stretch located respectively. Presence of oxygen-containing groups confirmed that the result of oxidation in the GO and results are also similar to previous studies [17]. Besides, after decoration with Ag NPs, compare with the spectrum of graphene oxide, the -OH groups became stretched out while the characteristic peak intensity of GO slightly decreased due to the interactions between Ag^+ ions and oxygen-containing groups on the GO sheets.

The crystallographic structure of synthesized Ag NPs-GO nanocomposites investigated from XRD pattern (Figure 2B). A sharp diffraction peak observed for GO around 11.7° corresponding to (001) plane. This result indicated that the successful preparation of GO and matched with references data. The XRD pattern observed for the Ag NPs-GO nanocomposite around 38.1° , 44.3° , 64.5° and 77.5° corresponding to the crystal lattice planes of (111), (200), (220) and (311) respectively. It confirmed that the face-centered cubic Ag nanoparticles (JCPDS no 04-0783) formed, respectively while the peak of GO not observed in the composite due to the metal-nanoparticles strongly interacted to the GO layers may lead to the sheeting the peak of graphene oxide. Moreover, the sharp peak of 38.1° confirmed that the pure crystalline nature of Ag nanoparticle formed in the Ag NPs-GO nanocomposites [16-24].

3.3 Electrocatalytic study of Ag NPs-GO nanocomposite

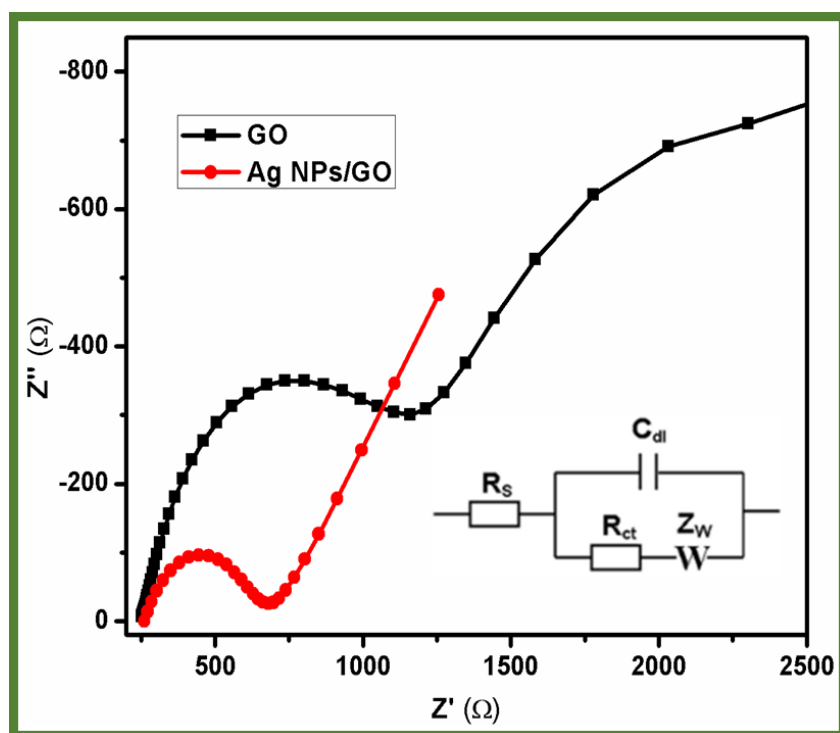


Figure 3. EIS curves of GO/SPCE (black) and Ag NPs-GO/SPCE (red)

The electrochemical impedance spectroscopy (EIS) is a convenient technique to calculate the electron transfer ability of the electrodes. (Figure 3) shows the EIS curve of GO/SPCE and Ag NPs-GO/SPCE modified electrode in 5mM $[\text{Fe}(\text{CN})_6]^{-3/-4}$ aqueous solution with 0.1 M KCl as a supporting electrolyte. The EIS data were plotted using the Randles circuit model (Inset: Figure 3) Where, R_{ct} , R_s , Z_w , and C_{dl} were depicted charge transmission resistance, electrolyte resistance, Warburg impedance and double layer capacitance, respectively. The subsequent order indicates that the diameter (D) of semicircles (i.e., R_{ct}); GO/SPCE (183 Ω) > Ag NPs/GO (97.3 Ω). Provided results show the lower resistance at Ag NPs-GO over other electrodes.

3.4 Electrochemical behavior of Ag NPs-GO modified electrode towards AA

The electrocatalytic ability of the Ag NPs-GO modified electrode towards AA was investigated by CV and the results compared with an unmodified SPCE (a), GO/SPCE (b) and Ag NPs-GO/SPCE modified electrode (c) in pH 7.0 containing 50 μM AA at a scan rate of 50 mV/s shown in (Figure 4A). The unmodified SPCE (a) does not show any apparent signal for AA, which indicates that the unmodified SPCE has poor electrocatalytic activity towards AA. The GO-SPCE modified electrode (b) shows a noticeable oxidative peak in the potential of 0.3853. An enhanced and well-defined oxidative peak current for AA was observed at Ag NPs-GO/SPCE electrode in the potential of 0.2699V.

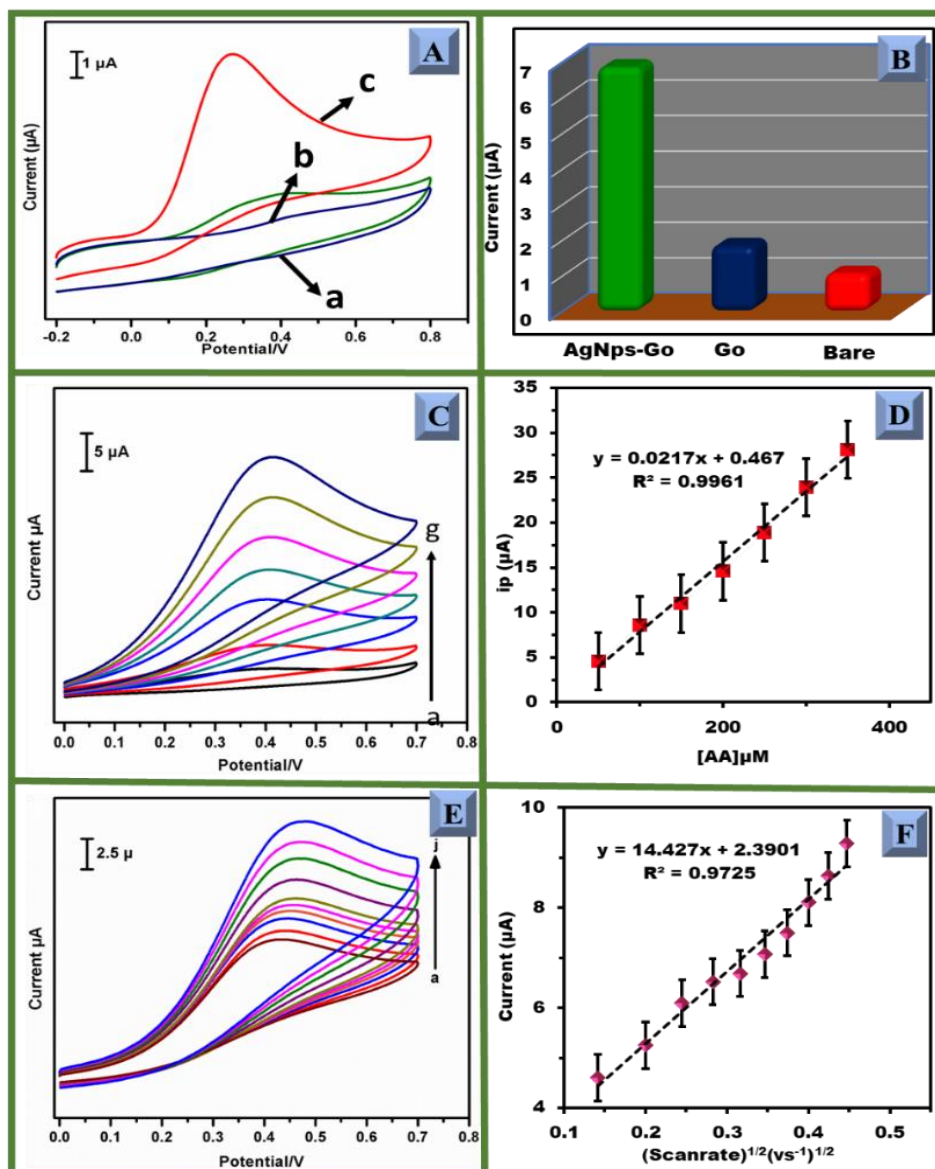


Figure 4. (A) CVs obtained at unmodified SPCE (a), GO/SPCE (b), and Ag NPs-GO/SPCE (c) in PB solution (pH 7.0) containing 50 μM AA, scan rate = 50 mV/s. (B) Corresponding peak current response / μA . (C) CVs Ag NPs-GO/SPCE in PB solution (pH 7.0) containing AA (50–350 μM), scan rate = 50 mV/s. (D) Calibration Plot of [AA]/ μM vs. response peak current/ μA . (E) CVs obtained at Ag NPs-GO/SPCE in PB solution (pH 7.0) containing 50 μM AA at different scan rate (20–200) mV/s. (F) (Scan rate) $^{1/2}$ (Vs $^{-1}$) $^{1/2}$ vs. Peak current (μA).

The corresponding peak current response is given in the (Figure 4B). We have also investigated the electrocatalytic behavior of Ag NPs-GO/SPCE toward detection of the different concentration of AA. (Figure 4C) CVs response of different concentration of AA (50–350) μM , into the PBS (7.0) at a scan rate of 50 mV/s. when adding 50 μM of AA oxidative peak current was observed in Ag NPs-GO/SPCE electrode. The oxidation peak of AA increases with the further increasing the AA concentration into the PBS, which indicates the typical electro-oxidation behavior of the composite modified electrode. The oxidation peak current of AA was plotted against the concentration of AA in (Figure

4D). The result also reveals that the Ag NPs-GO composite exhibit excellent electrochemical behavior towards detection of AA.

(Figure 4E) The effect of scan rate on the electrochemical response of AA at the Ag NPs-GO modified electrode. It is observed that the oxidation peaks current of AA increases linearly with increasing the scan rate from 20 to 200 mV s^{-1} . The oxidation peak current of AA was plotted against the square root of scan rate shown in (Figure 4F).

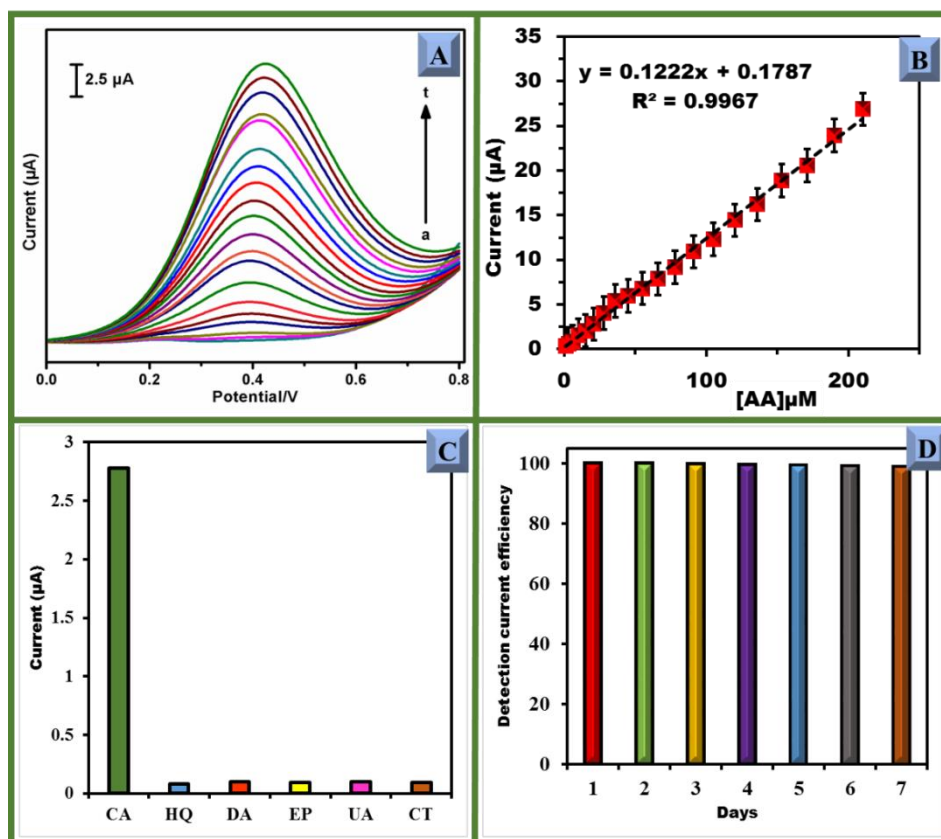


Figure 5. (A) DPV responses of Ag NPs-GO modified electrode towards different concentration of AA (1-210 μM) into PB solution (pH 7.0). (B) linear Plot of [AA]/ μM vs. response peak current/ μA . (C) selectivity of Ag NPs-GO sensor: plot between response current versus addition of 50 μM AA (a) and 1 mM additions of hydroquinone (HQ), dopamine (DA), epinephrine (EP), uric acid (UA) and catechol (CT) in PB solution (pH 7.0). (D) The CVs of Ag NPs-GO/SPCE towards 50 μM AA in 0.1 M PBS (Ph 7.0), monitored for the 7 days

3.5 Differential pulse voltammetry Determination of AA

(Figure 5A). shows the DPV response of Ag NPs-GO nanocomposite by varying concentration of AA. The modified electrode exhibited sharp DPV response for different concentration of AA (1 μM - 210 μM) and the calibration plot between AA concentration and DPV current response (Figure 5B). For AA, the regression equation (I) was obtained as,

$$[I_{pa}]/\mu\text{A} = 0.1222 [AA]/(\mu\text{A } \mu\text{M}^{-1}) + 0.1787 \quad (\text{I})$$

The linear plot revealed good linearity with the slope of $0.997 \mu\text{A } \mu\text{M}^{-1} \cdot \text{cm}^{-2}$. The sensitivity ($1.71 \mu\text{A } \mu\text{M}^{-1} \text{ cm}^{-2}$), and limit of detection (25 nM). The linear range, LOD, and sensitivity of Ag NPs/GO nanocomposite modified SPCE are comparable with previously reported articles (Table 1).

Table 1. Comparison of Sensor Parameters of LOD and linear range for the Detection of AA at Ag NPs-GO Nanocomposite Modified electrode with previously Reported Works.

Modified Electrode	LOD (μM)	Linear Range (μM)	Method	Ref.
^a RGO-ZnO/ ^b GCE	3.71	50–2350	DPV	[11]
^c Au/RGO/GCE.	0.051	0.24 to 1.5	DPV	[25]
^d MWCNT/ ^e CCE	7.71	15–800	DPV	[27]
^f Au-PANI	8.2	10–1200	AMP	[28]
IrOx nanofibers	0.4	1–1000	AMP	[12]
^h PImox- ⁱ GO/GCE	18	75–2275	DPV	[29]
^j AuNCs/ ^k AGR/MWCNT/GCE	0.27	10-150	SWV	[30]
^l H-GO/GCE	0.3	1.0–100	DPV	[31]
^m CTAB-GO/MWNT/GCE	1.0	5.0–300	DPV	[32]
ⁿ PdPt/RGO/GCE	0.61	40–1200	DPV	[33]
^o BN/GCE	3.77	30–1000	DPV	[1]
^p e-FGPE	2	20–400	DPV	[34]
Ag NPs-GO /SPCE	0.025	1-210	DPV	This work

^aReduced graphene oxide, ^bglassy carbon electrode, ^cmulti walled carbon nanotube gold particle, Carbon Ceramic Electrode, ^fgold nanoparticle, ^gscreen printed carbon electrode, ^hoveroxidized polyimidazole, ⁱgold nanoclusters, ^kactivated graphene, ^lhemin, ^mhexadecyl trimethyl ammonium bromide, ^oBoran nitrite, ^pexfoliated flexible graphite paper.

3.6 Interference, reproducibility, and stability of Ag NPs-GO sensor

To evaluate the anti-interference ability of Ag NPs-GO/SPCE, several electrochemical active interferents namely, hydroquinone (HQ), epinephrine (EP), uric acid (UA), dopamine (DA), and catechol (CT) were examined at Ag NPs-GO modified electrode. There is no additional peak observed for the above-mentioned interfering biomolecules and also exhibit an excellent current response to each addition of AA, revealing superior selectivity of Ag NPs-GO/SPCE (Figure 5C). To assess the reproducibility of the Ag NPs-GO modified electrode for the AA detection, 5 successive measurements carried out the with the same electrode. The relative standard deviations (RSD) calculated to be 3.65%. The results revealed that the good reproducibility of the developed Ag NPs-GO/SPCE electrode. The stability of biosensor is significant importance for the practical application. The stability of the Ag NPs-GO/SPCE was investigated by conducting the experiment with continuous use the same modified electrode for 7 days. After 7 days, the peak current intensity only decayed by

less than 2% of the initial intensity, revealing a good storage stability of Ag NPs-GO/SPCE (Figure 5D). Thus, the as-developed Ag NPs-GO/SPCE could serve as a sensitive, selective and stable biosensor for the detection of AA.

Table 2. Determination of AA in real samples using Ag NPs/GO/SPCE

Real Samples	Ascorbic acid			
	Added/ μM	Found/ μM	Recovery/%	*RSD/%
Human urine sample	5	4.93	98.6	3.01
	5	9.84	98.4	3.22
Vitamin C tablet	5	4.85	97.0	3.24
	5	9.67	96.7	2.80

* Related standard deviation (RSD) of 3 independent experiments

3.7 Real sample analysis

The practical applicability of the Ag NP-GO/SPCE verified in the real sample such as human urine and vitamin c tablet using the standard addition technique. It was found that the recovery results observed for human urine samples and vitamin C tablet ranged between 98.5% and 96.7% respectively, indicating that the Ag NPs-GO/SPCE could be used for the determination of AA in real samples. The results are summarized in Table 2.

4. CONCLUSIONS

In summary, a simple, inexpensive and disposable screen-printed carbon electrode (SPCEs) was used to developed Ag NPs-GO modified sensor for the ascorbic acid detection. The synthesis approach involves cost effective ultra-sonication method for Ag NPs decorated on GO without any functionalization step. The oxidation peaks current observed in the Ag NPs-GO composite based ascorbic acid sensor was ~6 folds greater than that of bare SPCE. The Ag NPs-GO sensor showed the lower limit of detection (25 nM), superior reproducibility, stability with a sensitivity of $1.71 \mu\text{A mM}^{-1} \text{cm}^{-2}$ ($R^2=0.9967$) in the linear range of 1–210 μM . The real samples such as human urine and vitamin C tablets were used to evaluate practical application of the proposed Ag NPs-GO sensor.

ACKNOWLEDGEMENTS

This work was supported by the National Science Council and the Ministry of Education of Taiwan (Republic of China) and National Taipei University of Technology, Taipei, Taiwan.

References

1. C.e. Zou, J. Zhong, S. Li, H. Wang, J. Wang, B. Yan, Y. Du, *J. Electroanal. Chem.*, 805 (2017) 110-119.
2. Y.-G. Lee, B.-X. Liao, Y.-C. Weng, *Chemosphere.*, 173 (2017) 512-519.
3. G. Darabdhara, B. Sharma, M.R. Das, R. Boukherroub, S. Szunerits, *Sens. Actuators, B.*, 238 (2017) 842-851.
4. Q. Li, C. Huo, K. Yi, L. Zhou, L. Su, X. Hou, *Sens. Actuators, B.*, (2018).
5. I. Sebarchievici, A. Lascu, G. Fagadar-Cosma, A. Palade, I. Fringu, M. Birdeanu, B. Taranu, E. Fagadar-Cosma, *C. R. Chim.*, (2017).
6. M.Y.A. Khan, M. Zahoor, A. Shaheen, N. Jamil, M.I. Arshad, S.Z. Bajwa, N.A. Shad, R. Butt, I. Ali, M.Z. Iqbal, *Mater. Res. Bull.*, n (2018).
7. L. Zhang, J. Feng, K.-C. Chou, L. Su, X. Hou, *J. Electroanal. Chem.*, 803 (2017) 11-18.
8. L. Fu, A. Wang, G. Lai, W. Su, F. Malherbe, J. Yu, C.-T. Lin, A. Yu, *Talanta.*, 180 (2018) 248-253.
9. P.L. dos Santos, V. Katic, K.C. Toledo, J.A. Bonacin, *Sens. Actuators., B* 255 (2018) 2437-2447.
10. R. Sha, S. Badhulika, *J. Electroanal. Chem.*, (2018).
11. X. Zhang, Y.-C. Zhang, L.-X. Ma, *Sens. Actuators, B* 227 (2016) 488-496.
12. S.-j. Kim, Y.L. Kim, A. Yu, J. Lee, S.C. Lee, C. Lee, M.H. Kim, Y. Lee, *Sens. Actuators, B.*, 196 (2014) 480-488.
13. M.A. Alonso-Lomillo, O. Domínguez-Renedo, A. Saldaña-Botín, M.J. Arcos-Martínez, *Talanta.*, 174 (2017) 733-737.
14. L. Zhang, G. Wang, D. Wu, C. Xiong, L. Zheng, Y. Ding, H. Lu, G. Zhang, L. Qiu, *Biosens. Bioelectron.*, 100 (2018) 235-241.
15. J.P. Bartolome, A. Fragoso, *Inorg. Chim. Acta.*, 468 (2017) 223-231.
16. Y. Liu, L. Wang, H. Zhang, F. Ran, P. Yang, H. Li, *RSC Adv.*, (64) (2017) 40119-40123.
17. T. Vi, S. Lue, *Mater. Sci. Eng.*, 2016, p. 012033.
18. O. Parkash, C.Y. Yean, R.H. Shueb, *Diagnostics.*, 4(4) (2014) 165-180.
19. K. Hareesh, J. Williams, N. Dhole, K. Kodam, V. Bhoraskar, S. Dhole, *Mater. Res. Express.*, 3 (7) (2016) 075010.
20. J. Tian, S. Liu, Y. Zhang, H. Li, L. Wang, Y. Luo, A.M. Asiri, A.O. Al-Youbi, X. Sun, *Inorg. Chem.*, 51(8) (2012) 4742-4746.
21. Y. Haldorai, B.-K. Kim, Y.-L. Jo, J.-J. Shim, *Mater. Chem. Phys.*, 143(3) (2014) 1452-1461.
22. K.R. Reddy, F. Alonso-Marroquin, *AIP Publishing.*, 2017, p. 020003.
23. A. Sudarvizhi, Z.A. Siddiqha, K. Pandian, *J Chem Applied Biochem* 1(1) (2014) 101.
24. C. Pérez-Ràfols, J. Bastos-Arrieta, N. Serrano, J.M. Díaz-Cruz, C. Ariño, J. De Pablo, M. Esteban, *Sensors.*, 17(6) (2017) 1458.
25. C. Wang, J. Du, H. Wang, C.e. Zou, F. Jiang, P. Yang, Y. Du, *Sens. Actuators, B.*, 204 (2014) 302-309.
J. Yan, S. Liu, Z. Zhang, G. He, P. Zhou, H. Liang, L. Tian, X. Zhou, H. Jiang, *Colloids Surf B.*, 111 (2013) 392-397.
26. B. Habibi, M.H. Pournaghi-Azar, *Electrochim. Acta.*, 55(19) (2010) 5492-5498.
H. Zhang, F. Huang, S. Xu, Y. Xia, W. Huang, Z. Li, *Electrochem. Commun.*, 30 (2013) 46-50.
27. X. Liu, L. Zhang, S. Wei, S. Chen, X. Ou, Q. Lu, *Biosens. Bioelectron.*, 57 (2014) 232-238.
28. Adel A. Abdelwahaba, Yoon-Bo Shimb, *Sens. Actuators, B.*, 221 (2015) 659-665
29. Hao Lin Zou, Bang Lin Li, Hong Qun Luo, Nian Bing Li, *Sens. Actuators., B* 207 (2015) 535-541

30. YuJunYang, WeikunLi, *Sens. Actuators.*, B 56(2014)300–306
31. Jun Yan, Shi Liu, Zhenqin Zhang, Guangwu He, Ping Zhou, Haiying Liang, Lulu Tian,
32. Xuemin Zhou, Huijun Jiang, *Colloids Surf B.*, 111 (2013) 392– 397
33. Weihua Caia, Ting Laia, Haijun Dub, Jianshan Ye, *Sens. Actuators*, B 193 (2014) 492– 500

© 2018 The Authors. Published by ESG (www.electrochemsci.org). This article is an open access article distributed under the terms and conditions of the Creative Commons Attribution license (<http://creativecommons.org/licenses/by/4.0/>).